Wiley
European Journal of Cancer Care
Volume 2024, Article ID 3735659, 19 pages
https://doi.org/10.1155/2024/3735659

WILEY

Research Article

Combining Gene Expression Data with GWAS Highlights the Causal Gene CCDC25 as a Biomarker for a Favorable Prognosis in Colorectal Cancer

Guowei Zhang,[1] Yuling Ma,[2] Jianfeng Shao,[3] Caiping Ke,[4] Chunhua Li,[5] and Yaping Dong[5]

[1]*Hepatobiliary Pancreatic and Hernia Surgery, Guangdong Second Provincial General Hospital, Guangzhou, China*
[2]*Internet Medical Center, Guangdong Second Provincial General Hospital, Guangzhou, China*
[3]*Department of Abdominal Pelvic Oncology, The First People's Hospital of Zhaoqing, Zhaoqing, China*
[4]*Department of Oncology, Maoming People's Hospital, Maoming, China*
[5]*Department of Oncology, The Second Affiliated Hospital of Shandong University of Traditional Chinese Medicine, Jinan, China*

Correspondence should be addressed to Chunhua Li; lchdoctor01@163.com and Yaping Dong; 772709788@qq.com

Received 21 May 2024; Accepted 2 July 2024

Academic Editor: Pranshu Sahgal

Background. Coiled-coil domain containing 25 (CCDC25) is a receptor for neutrophil extracellular trap (NET) DNA and is involved in various cancers, including CRC. This study aimed to investigate the regulatory role of CCDC25 in CRC using GWAS data, eQTL, transcriptomic profiles, and clinical information of CRC patients. *Methods*. From open-source databases, GWAS summary data, eQTL expression profiles, and transcriptomic profiles, as well as clinical information were collected for CRC patients. Mendelian randomization (MR) was used to investigate the causal relationship between CCDC25 and CRC risk. The expression of CCDC25 and its associated differentially expressed genes (DEGs) were identified. We explored the relationship between CCDC25 expression and survival, biological functions, immune cell infiltration, immune checkpoint expression, and response to immunotherapy. *Results*. High CCDC25 expression reduces the risk of CRC. CCDC25 is downregulated in various cancers, particularly in CRC tumor tissues compared to normal tissues. Metabolic pathways are enriched in groups with high CCDC25 expression, while cancer-related pathways are enriched in groups with low CCDC25 expression. High CCDC25 expression is also associated with increased infiltration of resting memory CD4+ T cells, elevated levels of most immune checkpoints, and an enhanced response to anti-PD1 therapy. In addition, 95 DEGs were identified between high-CCDC25 and low-CCDC25 groups, and eight genes (FDFT1, ASAH1, ADAM9, CXCL14, SERPINA1, NAT1, EREG, and GSR) were identified as prognostic genes. *Conclusion*. CDC25 might serve as a candidate diagnostic and prognostic marker for CRC patients.

1. Introduction

In 2020, there will be more than 1.9 million new cases of colorectal cancer (CRC) and 935,000 deaths as a result of this cancer [1]. The incidence patterns of CRC are similar between sexes but vary by age [2]. In the older population, CRC incidence has declined, but in the younger population, it has steadily increased. Diagnoses in younger individuals are expected to rise further in the next decade [3]. An aging population, lifestyle factors, obesity, and smoking increase the risk of CRC [4]. A number of treatments are available for CRC, including endoscopic and surgical excision, radiotherapy, systemic therapy, local ablative therapy, palliative chemotherapy, targeted therapy, and immunotherapy [4]. Microsatellite instability (MSI) is crucial for predicting differential treatment response and prognosis in CRC patients [5]. In studies, it has been found that immunotherapy is more likely to be effective when there is high microsatellite instability (MSI-H) [6]. While these therapeutic options have contributed to improving overall survival for advanced

patients, however, it is noteworthy that more than 70% of metastatic patients survive beyond 1 year, over 30% beyond 3 years, and less than 20% beyond 5 years [7]. As the diseases only become symptomatic at an advanced stage, early detection is crucial for reducing morbidity and mortality from CRC.

CCDC25 is found on human chromosome 8p21.1 and is expressed by a variety of mammalian cells [8]. In recent years, CCDC25 has been widely found in several tumors; however, it reveals the dual roles in different types of tumors [9]. For example, CCDC25 has been recognized as a receptor of neutrophil extracellular trap (NET) DNA, facilitating the binding with surrounding NET-DNA and promoting NET formation. In addition, CCDC25 overexpression in primary breast cancer cells has been associated with reduced metastasis-free survival [10]. CCDC25 overexpression has been shown to be linked with poor overall survival in cholangiocarcinoma and hepatocellular carcinoma (HCC) [11, 12]. However, the regulatory role of CCDC25 in CRC remains uncertain.

Mendelian randomization (MR) is an innovative epidemiological analysis method which is used to investigate the causal relationship between risk factors and outcomes by leveraging genetic variants [13]. Compared with traditional observational studies, the MR method has the advantage of avoiding the influence of confounding factors and eliminating the interference of reverse causality [14]. A MR analysis has indicated that the increased level of plasma ABO protein is related to the increased risk of coronavirus disease 2019 (COVID-19) [15]. We also found no correlation between serum bilirubin level and risk of heart failure in either the European or East Asian population by MR analysis [16]. However, there is still no evidence that supports the casual association between CCDC25 and the risk of CRC.

In the present study, we initially explored the causal association between CCDC25 and the risk of CRC using MR analysis. Subsequently, we conducted a comprehensive analysis of the role of CCDC25 in CRC progression and prognosis, utilizing gene expression profiles and clinical information of CRC patients.

2. Methods

2.1. GWAS Summary Data Source. In the present study, a two-sample MR study was conducted to determine the association of CCDC25 levels with the risk of CRC. This analysis was based on the expression quantitative trait loci (eQTL) data of CCDC25 and the GWAS summary statistics for CRC outcomes (Figure 1(a)). Exposure data source: the eQTL data used in our study were extracted from the eQTLGen consortium (https://www.eqtlgen.org/cis-eqtls.html) which were conducted on peripheral blood samples collected from a total of 31,684 individuals [17], and the top associated cis-eQTLs were selected according to the following thresholds: P value $<5\times10^{-8}$ and false discovery rate (FDR) <0.05 within a range of ±100 kb windows. Outcome data source: the GWAS summary statistics for CRC outcomes were obtained from the publicly available database IEU Open GWAS (https://gwas.mrcieu.ac.uk/datasets/ebi-a-GCST012876/) [18] and contains 26,554 cases and 11,895 controls. All participants included in this study were of European ancestry only.

2.2. Selection of Genetic Instrument Variables (IVs). IVs were selected based on three assumptions: (i) IVs must have a strong association with the exposure; (ii) IVs should be independent of other confounding factors between the relationship, exposure, and outcome; and (iii) IVs should influence outcome solely through the exposure [19]. Here, single-nucleotide polymorphisms (SNPs) were chosen as IVs based on the following criteria: meeting a genome-wide significance threshold of $P<5\times10^{-8}$ and a false discovery rate (FDR) <0.05, having a minor allele frequency (MAF) >0.01, and exhibiting no linkage disequilibrium (LD: $r^2<0.1$) within a 10,000 kb clumping window [20]. In addition, the selected SNPs had an F-statistic ($\text{beta}^2/\text{se}^2$) >10 [21]. The direction of the SNPs was determined using the Steiger filtering test.

2.3. TwoSample MR Analysis. In the present study, the "TwoSampleMR" package in R was utilized to assess the causal relationship between CCDC25 and the risk of CRC using several methods: inverse-variance weighted (IVW), weighted median, MR-Egger regression, MR robust adjusted profile score (MR-RAPS), and MR-pleiotropy residual sum and outlier (MR-PRESSO) methods. The IVW method served as the primary approach for MR estimation, employing a meta-analysis of Wald ratios from effective SNPs. [22]. The weighted median method was applied to maintain consistent effect estimates even if more than 50% of selected genetic variants were invalid instruments [23]. MR-Egger regression, which considers the MR-Egger intercept to detect and adjust for bias from pleiotropy, was also employed as an additional method for causal inference [24]. MR-RAPS is a robust method that tests the causal relationship by overcoming the weak instrumental variables and enhances the statistical power [25]. MR-PRESSO is a method that can detect the outliers of IVs and adjust the horizontal pleiotropy [26]. Furthermore, Cochran's Q-test and Steiger filtering methods were employed in this study to assess heterogeneity and confirm the directionality of the IVs. Leave-one-out analysis was used to evaluate the robustness of causal estimation by systematically removing each included SNP to correct the bias caused by outliers [13].

2.4. Bulk RNA-Seq Data Acquisition and Processing. mRNA expression data and corresponding clinical data of the TCGA-COAD cohort, containing 453 tumor samples and 41 nontumor samples, were obtained from The Cancer Genome Atlas (TCGA, https://cancergenome.nih.gov) and used as a training cohort. For CRC patients, tumor gene mutation MAF also was downloaded from TCGA. Besides, mRNA expression data and corresponding clinical data from GSE41258, GSE29623, and GSE159216 datasets were downloaded from Gene Expression Omnibus (GEO, https://www.ncbi.nlm.nih.gov/geo/) and used as external validation

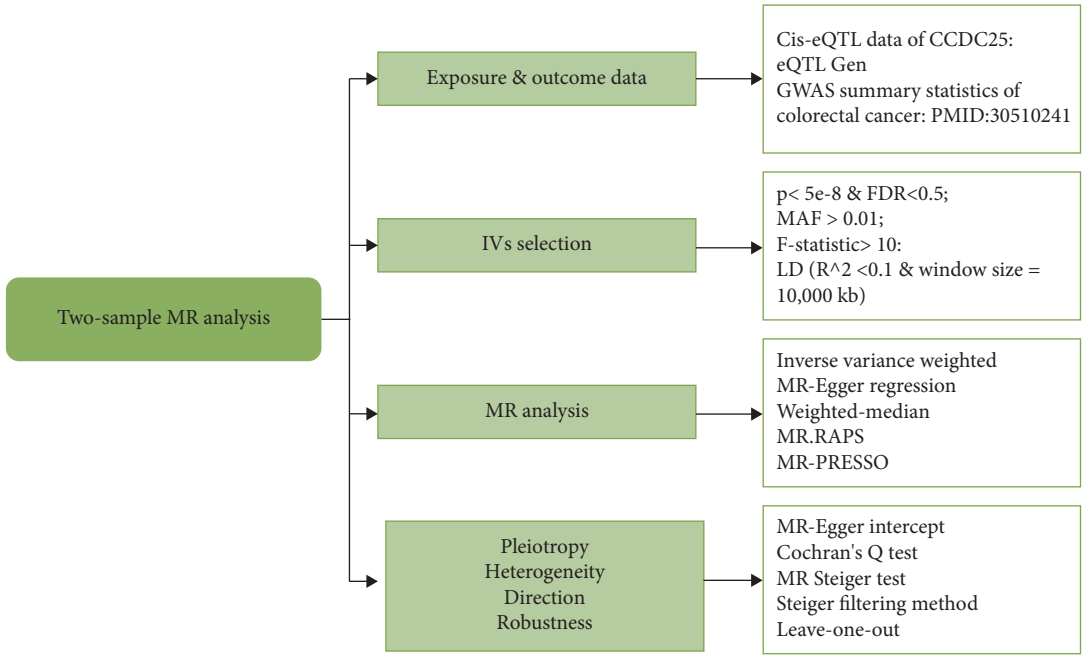

(a)

Gene	Outcome	nSNPs	Method	OR (95%CI)	P−value	Q	Q_pval	intercept	Pleiotropy_Pval
CCDC25	CRC	18	IVW	0.90 (0.83, 0.97)	0.006	11.1	0.849		
CCDC25	CRC	18	MR−Egger	0.92 (0.77, 1.09)	0.352			−0.004	0.775
CCDC25	CRC	18	Weighted median	0.90 (0.81, 1.00)	0.042				
CCDC25	CRC	18	MR−RAPS	0.89 (0.82, 0.97)	0.005				

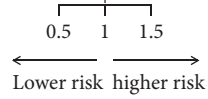

(b)

Figure 1: Continued.

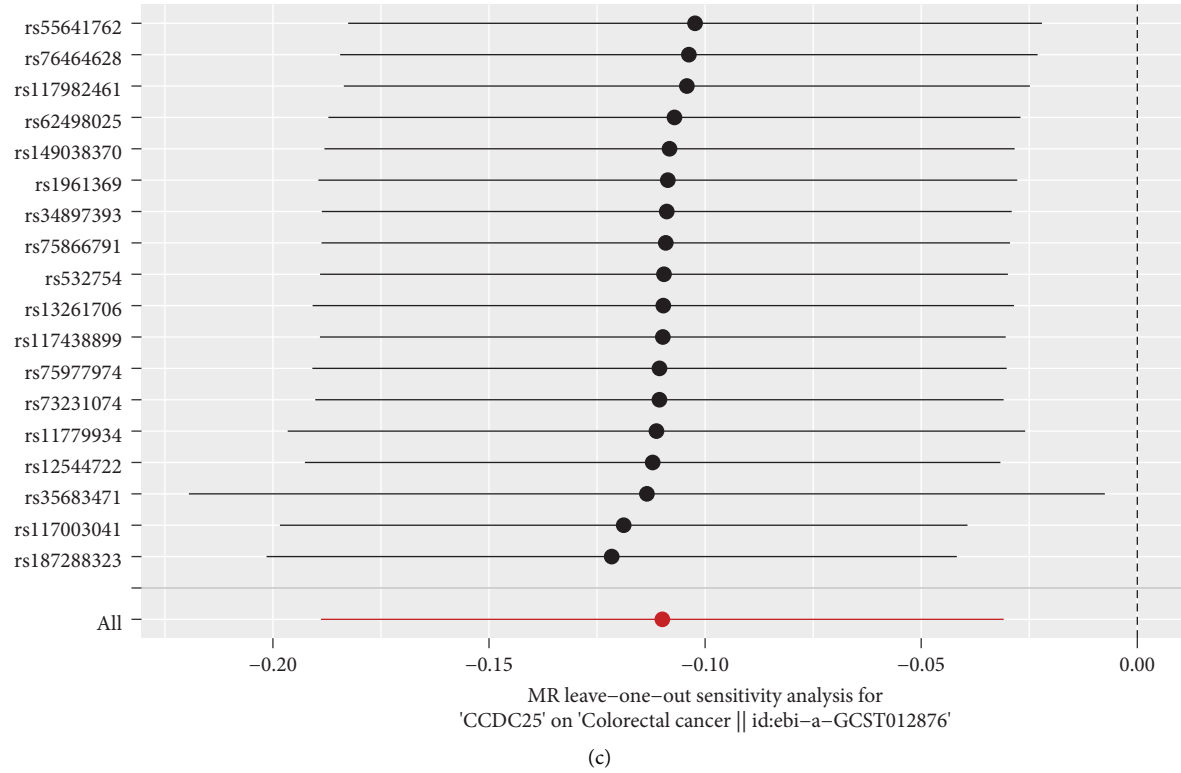

Figure 1: The causal role of CCDC25 was significantly negatively associated with the risk of CRC. (a) The work flowchart of the MR analysis. (b) Forest plots of the results for the IVW, MR-Egger, weighted median, and MR-RAPS analyses. (c) Forest plot of MR leave-one-out sensitivity analysis.

cohorts. GSE41258, GSE29623, and GSE159216 datasets were generated by GPL96, GPL570, and GPL17586 platforms, respectively.

2.5. Differential Expression of CCDC25. The differentially expressed CCDC25 in pan-cancer was determined based on the TIMER database (https://timer.cistrome.org/) [27]. The statistical significance of differential expression in the tumors compared to normal tissues for each cancer type was evaluated using the Kruskal–Wallis test with the threshold of the fold change (FC) of 1.0 and P value of <0.05. The differentially expressed genes (DEGs) between tumor samples and nontumor samples were screened using the "limma" package in R with a P value of <0.05. The expression of CCDC25 was identified from those DEGs.

2.6. Correlation between CCDC25 and Overall Survival and Clinicopathological Characteristics in CRC. To assess the prognostic significance of CCDC25 in CRC, patients were stratified into high- and low-CCDC25 expression groups based on an optimal cutoff value derived from CCDC25 expression levels in CRC. Overall survival (OS) analysis for CRC patients was conducted using Kaplan–Meier methods implemented with the "survminer" R package. The correlation between CCDC25 expression and clinical characteristics such as age, gender, MSI status, and clinical stage was evaluated using the Kruskal–Wallis test.

2.7. Screening of the Differentially Expressed Genes (DEGs) between High- and Low-CCDC25 Groups. The DEGs between high-CCDC25 and low-CCDC25 groups were screened using the "limma" package in R with $|\log2\ (FC)| > 0.585$ and P value of <0.05. All DEGs between high-CCDC25 and low-CCDC25 groups were visualized in volcano plots using the "ggplot" package in R.

2.8. Gene Set Enrichment Analysis. We obtained 50 human cancer hallmarks (h.all.v7.4.symbols.gmt) from Molecular Signatures Database (MSigDB, https://www.gsea-msigdb.org/gsea/msigdb/). Subsequently, we conducted gene set enrichment analysis (GSEA, https://www.gsea-msigdb.org/gsea/index.jsp) to explore whether genes differentially expressed between high-CCDC25 and low-CCDC25 expression groups were enriched in biologically significant processes [28]. The significance was determined using the Kruskal–Wallis test.

2.9. Evaluation of Immune Cell Infiltration. The "IOBR" package in R, incorporating TIMER, ESTIMATE, xCell, and CIBERSORT algorithms, was utilized in this study. Specifically, the CIBERSORT algorithm was employed to analyze gene expression patterns and identify the proportions of 22 immune cell types within samples. This analysis was based on differentially expressed genes (DEGs) identified between the high-CCDC25 and low-CCDC25 expression groups. The

Kruskal–Wallis test was then used to assess differences in the compositions of immune cell types between these two groups.

2.10. Identification of Differentially Expressed Immune Checkpoints and Immunotherapy Response. The differentially expressed 46 immune checkpoints (BTN3A1, CD226, CD27, CD28, CD40, CD40LG, CD70, CD96, CEACAM1, ICOS, ICOSLG, IL2RA, KIR2DL4, TNFRSF12A, TNFRSF18, TNFRSF4, TNFRSF9, TNFSF14, TNFSF18, TNFSF4, TNFSF9, ADORA2A, BTLA, BTN2A2, CD160, CD200, CD200R1, CD276, CD47, CTLA4, HAVCR2, IDO1, KIR2DL1, KIR2DL3, KIR3DL1, KIR3DL2, KIR3DL3, LAG3, LAIR1, LGALS3, LGALS9, PDCD1, SIRPA, TDO2, TIGIT, and VTCN1) between high-CCDC25 and low-CCDC25 groups were determined using the Kruskal–Wallis test. The possible response to immunotherapy was predicted using the Submap method from GenePattern (https://cloud.genepattern.org/gp/pages/index.jsf).

2.11. Construction and Validation of a CCDC25-Related Risk Model. In this study, several analyses and validations were conducted using R packages: univariate Cox proportional hazards regression analysis: we utilized the "survival" package to identify overall survival (OS)-related differentially expressed genes (DEGs), with a cutoff P value of <0.05. LASSO Cox regression analysis: we employed the "glmnet" package to perform the least absolute shrinkage and selection operator (LASSO) Cox regression. This step aimed to identify a prognostic gene signature, where regression coefficients (β) were derived. The CCDC25-related risk score for each sample was calculated by using the following formula: risk score = $\sum_{i=1}^{n}$coef (genei) ∗ expr (genei), where coef represents the regression coefficient and expr represents the gene expression level. Risk stratification: patients within the TCGA-COAD cohort were stratified into high-risk and low-risk groups based on the median values of the risk score derived from LASSO Cox regression. Overall survival (OS) analysis: OS curves were generated using the Kaplan–Meier method to evaluate survival differences between the high-risk and low-risk groups. Time-dependent ROC curves: using the "survivalROC" package, time-dependent ROC curves were plotted for 1-year, 3-year, and 5-year intervals to assess the predictive accuracy of the prognostic model. External validation: external cohorts (GSE41258, GSE29623, and GSE159216 datasets) were utilized to validate the prognostic model developed from the TCGA-COAD cohort. These steps collectively aimed to identify and validate a robust prognostic model for CRC based on CCDC25-related gene signatures and risk scores.

2.12. Development and Evaluation of a Predictive Nomogram. Further investigation into the independence of the predictive prognostic model from conventional clinical characteristics involved several analyses: multivariate Cox proportional hazards regression analysis: this analysis aimed to identify independent factors affecting survival using the "survival" package in R. Nomogram construction. Based on the results of the multivariate Cox analysis, a nomogram was constructed to predict survival time for CRC patients, integrating both clinical characteristics and the prognostic gene signature. Time-dependent ROC curves: ROC curves for 1-year, 3-year, and 5-year survival predictions were generated using the "survivalROC" package to assess the accuracy of the predictive model. Area under the ROC curve (AUC): the AUC values from the ROC curves were calculated to quantitatively evaluate the discriminatory ability of the prognostic model. Decision curve analysis (DCA): DCA was performed to assess the clinical utility and outcome of different decision strategies based on the nomogram predictions. These analyses collectively aimed to validate and demonstrate the clinical relevance and independence of the developed prognostic model for CRC patients.

2.13. Statistical Analysis. All analyses were performed in R software in this study. "TwoSampleMR" version 0.5.7, "MR-PRESSO" version 1.0, and "forestplot" version 3.1.3 packages in R were used to conduct MR analysis. "survival" version 3.5-3, "ggplot2" version 3.4.1, "pheatmap" version 1.0.12, "estimate" version 1.0.13, "limma" version 3.54.1, "GSEA" version 4.2.2, "glmnet" version 4.1-2, "timeROC" version 0.4, "survminer" version 0.4.9, and "tidyverse" version 1.3.2 packages in R were used to perform the transcriptomic data analysis. P value <0.05 was considered statistically significant.

3. Results

3.1. Causal Role of CCDC25 in CRC Risk. Eighteen SNPs significantly associated with CCDC25 ($P < 5 \times 10^{-8}$; FDR <0.05; MAF >0.01; LD: $r^2 < 0.1$; F-statistic >10) were selected (Table 1). The causal relationship between CCDC25 and CRC risk was investigated using MR analysis. As depicted in Figure 1(b), IVW analysis indicated a negative association between high CCDC25 expression and CRC risk (OR: 0.90; 95% CI: 0.83–0.97; $P = 0.006$). Results from the weighted median and MR-RAPS methods were consistent (weighted median: OR: 0.90; 95% CI: 0.81–1.00; $P = 0.042$; MR-RAPS: OR: 0.89; 95% CI: 0.82–0.97; $P = 0.005$). Further assessments showed no significant heterogeneity (Cochran's Q statistic; Q_P value >0.05) or horizontal pleiotropy (MR-Egger intercept; pleiotropy_P value >0.05). MR-PRESSO results supported IVW findings, confirming no outliers (OR: 0.90; 95% CI: 0.84–0.97; $P = 0.004$; Table 2). The Steiger filtering test confirmed consistent SNP directions (Table 3). In addition, leave-one-out analysis demonstrated the robustness of MR results (Figure 1(c)). Collectively, these findings suggest that high CCDC25 expression may inhibit CRC risk.

3.2. Differential Expression of CCDC25 in CRC. Following our MR analysis indicating a causal link between CCDC25 and CRC risk, we explored CCDC25 expression across various cancers using TIMER 2.0 (https://timer.cistrome.org/) based on TCGA clinical data. We observed

Table 1: Information of the selected SNPs in eQTLGen for MR analysis.

Gene	SNP	Chr	Position	Effect allele	Other allele	EAF	Beta	SE	*P* value	Sample size	R^2 (%)	*F*-statistic
CCDC25	rs117003041	8	27625808	A	G	0.027	−0.204	0.028	$2.1E-13$	24545	0.22	54
CCDC25	rs117438899	8	27628519	A	G	0.054	0.102	0.018	$1.0E-08$	30874	0.11	33
CCDC25	rs11779934	8	27700973	T	C	0.477	0.169	0.008	$3.6E-101$	31565	1.42	456
CCDC25	rs117982461	8	27557738	G	A	0.026	0.159	0.026	$1.1E-09$	28673	0.13	37
CCDC25	rs12544722	8	27587116	C	T	0.025	−0.253	0.028	$1.3E-19$	25874	0.32	82
CCDC25	rs13261706	8	27635617	T	C	0.065	−0.197	0.016	$3.1E-33$	30406	0.47	144
CCDC25	rs149038370	8	27573786	T	C	0.015	0.309	0.042	$2.3E-13$	18390	0.29	54
CCDC25	rs187288323	8	27707690	A	G	0.022	−0.235	0.031	$1.6E-14$	25154	0.23	59
CCDC25	rs1961369	8	27549870	C	A	0.476	0.096	0.008	$2.2E-33$	31569	0.46	145
CCDC25	rs34897393	8	27681643	G	A	0.024	0.259	0.028	$3.3E-20$	26547	0.32	85
CCDC25	rs35683471	8	27636729	T	C	0.332	0.316	0.008	$1.0E-200$	31569	4.42	1459
CCDC25	rs532754	8	27526345	G	C	0.314	0.059	0.009	$1.1E-11$	31058	0.15	46
CCDC25	rs55641762	8	27693576	C	A	0.038	−0.186	0.021	$7.3E-19$	31163	0.25	79
CCDC25	rs62498025	8	27625840	T	G	0.051	−0.183	0.018	$1.5E-23$	30407	0.33	100
CCDC25	rs73231074	8	27550775	C	A	0.018	0.227	0.033	$5.7E-12$	25523	0.19	47
CCDC25	rs75866791	8	27658995	C	T	0.022	0.209	0.029	$3.5E-13$	28229	0.19	53
CCDC25	rs75977974	8	27633237	A	G	0.072	−0.168	0.016	$9.5E-27$	30077	0.38	115
CCDC25	rs76464628	8.00	27631511	G	A	0.042	0.246	0.020	$5.0E-34$	30506	0.48	148

SNP, single-nucleotide polymorphism; Chr, chromosome; EAF, effect allele frequency; beta, effect value; SE, standard error of β; R^2, the extent to which instrumental variables explain exposure; *F*, *F*-statistic.

Table 2: MR-PRESSO analysis of the pleiotropy in the causality of CCDC25 and risk of CRC.

Gene	Outcome	MR-PRESSO	OR (95% CI)	*P* value
CCDC25	CRC	Raw	0.90 (0.84, 0.96)	0.004
CCDC25	CRC	Outlier corrected		

predominantly lower CCDC25 expression in solid tumor tissues compared to normal tissues across multiple cancers, including bladder cancer (BLCA), breast cancer (BRCA), colon cancer (COAD), kidney chromophobe (KICH), kidney clear cell carcinoma (KIRC), kidney papillary cell carcinoma (KIRP), liver cancer (LIHC), lung adenocarcinoma (LUAD), prostate cancer (PRAD), thyroid cancer (THCA), and endometrial cancer (UCEC). In addition, CCDC25 expression was lower in HPV- compared to HPV + head and neck cancer (HNSCC) and in nonmetastatic melanoma compared to metastatic melanoma (SKCM) (Figure 2(a)). Subsequently, we analyzed expression and clinical data from the TCGA database (https://cancergenome.nih.gov) to investigate CCDC25 expression in the TCGA-COAD cohort (Figure 2(b), Table S1). We identified 12,974 DEGs, with 7,111 upregulated and 5,863 downregulated genes in tumor tissues compared to normal tissues in the TCGA-COAD cohort ($|\log2\ (FC)| > 0.585$; P value <0.05). Furthermore, our analysis revealed that high CCDC25 expression correlates with longer survival in the TCGA-COAD cohort (Figure 2(c)). High CCDC25 expression was also positively associated with microsatellite instability (MSI) status and early clinical stages (Figures 2(d), 2(e), 2(f), and 2(g)), suggesting a potential association with favorable prognosis. These findings underscore the potential prognostic value of CCDC25 in CRC and highlight its differential expression patterns across various cancer types.

3.3. CCDC25-Associated Functional Annotation and Pathway Enrichment Analysis in CRC. We next explored the DEGs between high-CCDC25 and low-CCDC25 groups, resulting in a total of 95 DEGs (64 upregulated and 31 downregulated, Table S2) identified between high-CCDC25 and low-CCDC25 groups (Figure 3(a)). To delve deeper into pathway alterations associated with CCDC25 expression, we conducted gene set enrichment analysis (GSEA) across all genes between these groups. Our analysis revealed that a high CCDC25 expression was associated with multiple metabolism-related pathways, including adipogenesis, androgen response, apoptosis, cholesterol homeostasis, E2F targets, fatty acid metabolism, G2M checkpoint, glycolysis, interferon-gamma response, mitotic signaling, MYC targets, oxidative phosphorylation, and p53 pathway (Figure 3(b)). In contrast, low CCDC25 expression was linked to pathways such as Hedgehog signaling, KRAS signaling down, myogenesis, Notch signaling, UV response, and beta-catenin signaling (Figure 3(c)). These data suggested that CCDC25 expression may play a role in tumor metabolism and highlight potential pathways influenced by CCDC25 in CRC.

3.4. CCDC25-Associated Immune Cell Infiltration and Immunotherapeutic Response in CRC. Given the crucial roles of immune cells in the tumor microenvironment, we investigated the relationship between CCDC25 and immune cell infiltration. Our analysis revealed that high CCDC25 expression is associated with enrichment of resting memory CD4+ T cells within the tumor microenvironment (Figures 4(a) and 4(b)). Moreover, we also found increased expression of BTN3A1, CD226, CD96, KIR2DL4, TNFRSF9, TNFSF9, CD200, CTLA4, IDO1, KIR2DL1, LGALS3, and TIGIT but decreased expression of TNFRSF12A and TNFRSF4 in the high-CCDC25 group compared with the low-CCDC25 group (Figures 4(c), 4(e), and 4(f)). Submap results indicated that the high expression of CCDC25 exhibited a more sensitive response to anti-PD1 therapy (Figure 4(g)). These results indicated that patients with high expression of CCDC25 may potentially derive greater benefits from immunotherapy. Patients with high expression of CCDC25 are advised to consider immunotherapy more extensively.

3.5. Construction and Validation of a CCDC25-Associated Prognostic Model of CRC. To further investigate the prognostic value of CCDC25 in CRC, we performed a univariate Cox analysis on the DEGs between high-CCDC25 and low-CCDC25 groups. As shown in Table S3, a total of 34 prognostic genes were screened and then incorporated into a LASSO regression to identify prognostic gene signatures. As a result, eight genes (FDFT1, ASAH1, ADAM9, CXCL14, SERPINA1, NAT1, EREG, and GSR) were selected as prognostic signature genes (Figures 5(a), 5(b), and 5(c)). Furthermore, the 435 patients were divided into high-risk ($n = 217$) and low-risk groups ($n = 218$) according to the risk score and calculated using the expression and coefficient of each gene (Figures 5(d), 5(e), and 5(f)). The survival analysis indicated that the high-risk group had worse survival outcomes compared to the low-risk group (Figure 5(g)). Meanwhile, the AUC values of ROC curves for 1-, 3-, and 5 years were 0.704, 0.676, and 0.681, respectively (Figure 5(h)). These data indicated the accurate prediction of the prognostic model. Moreover, the external cohorts, including GSE41258, GSE29623, and GSE159216, were selected to perform the external validation. The survival analyses indicated that the patients in the high-risk group exhibited a worse survival time compared with the low-risk group (Figures 6(a), 6(b), 6(c), 6(d), 6(e), 6(f), 6(g), 6(h), and 6(i)). The ROC curves were drawn to validate the accuracy of the prognostic model (Figures 6(j), 6(k), and 6(l)).

Table 3: MR Steiger filtering method to assess the causal direction of each of the extracted SNPs on the expression of CCDC25 and CRC outcomes.

SNP	Gene	Outcome	rsq.exposure	Effective_n.exposure	rsq.outcome	Effective_n.outcome	Steiger_direction	Steiger_pval
rs117003041	CCDC25	Colorectal cancer	0.002193203	24545	$8.76541E-05$	26554	True	$2.2825E-05$
rs117438899	CCDC25	Colorectal cancer	0.001062091	30874	$3.09527E-06$	26554	True	0.000228849
rs11779934	CCDC25	Colorectal cancer	0.014241207	31565	$3.43266E-05$	26554	True	$1.08038E-42$
rs117982461	CCDC25	Colorectal cancer	0.001296527	28673	0.000106535	26554	True	0.00254848
rs12544722	CCDC25	Colorectal cancer	0.003164596	25874	$2.15866E-06$	26554	True	$3.42776E-10$
rs13261706	CCDC25	Colorectal cancer	0.00472195	30406	$1.58318E-05$	26554	True	$1.16293E-14$
rs149038370	CCDC25	Colorectal cancer	0.002912728	18390	$1.71702E-05$	26554	True	$2.00592E-07$
rs187288323	CCDC25	Colorectal cancer	0.002338336	25154	$8.82955E-05$	26554	True	$9.33692E-06$
rs1961369	CCDC25	Colorectal cancer	0.004572179	31569	$1.97008E-05$	26554	True	$2.97351E-14$
rs34897393	CCDC25	Colorectal cancer	0.003183788	26547	$1.20627E-05$	26554	True	$1.01144E-09$
rs35683471	CCDC25	Colorectal cancer	0.044169005	31569	0.000114536	26554	True	$8.4288E-131$
rs532754	CCDC25	Colorectal cancer	0.001483437	31058	$6.28916E-06$	26554	True	$1.63116E-05$
rs55641762	CCDC25	Colorectal cancer	0.002518379	31163	$8.55936E-05$	26554	True	$9.30193E-07$
rs62498025	CCDC25	Colorectal cancer	0.003277236	30407	$2.78352E-05$	26554	True	$5.83666E-10$
rs73231074	CCDC25	Colorectal cancer	0.001855052	25523	$1.82188E-06$	26554	True	$1.91467E-06$
rs75866791	CCDC25	Colorectal cancer	0.001871748	28229	$9.50336E-06$	26554	True	$2.56325E-06$
rs75977974	CCDC25	Colorectal cancer	0.003796547	30077	$6.30679E-06$	26554	True	$2.09594E-12$
rs76464628	CCDC25	Colorectal cancer	0.004825691	30506	$6.08621E-05$	26554	True	$1.83386E-13$

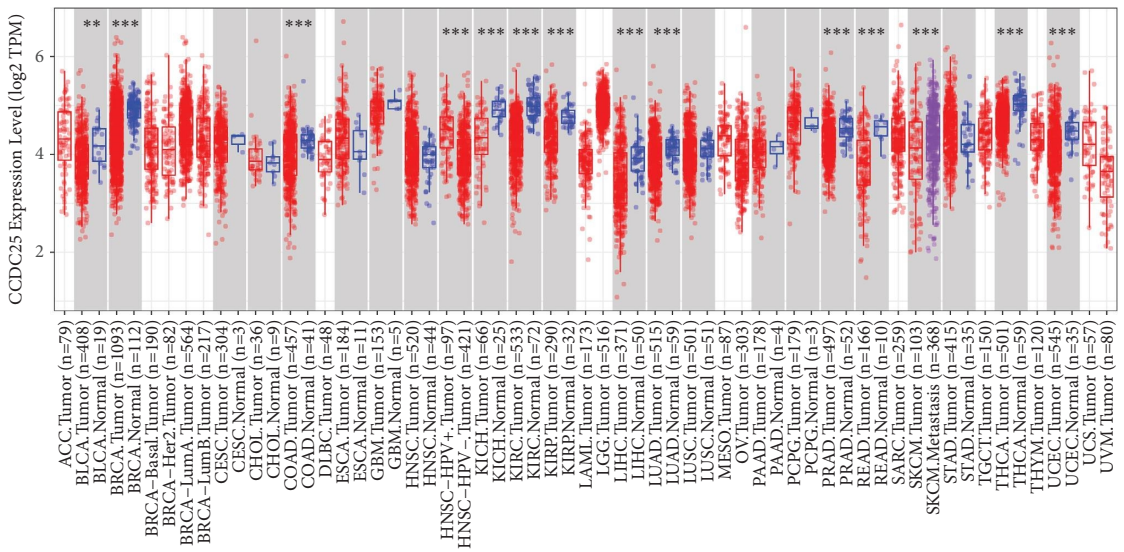

(a)

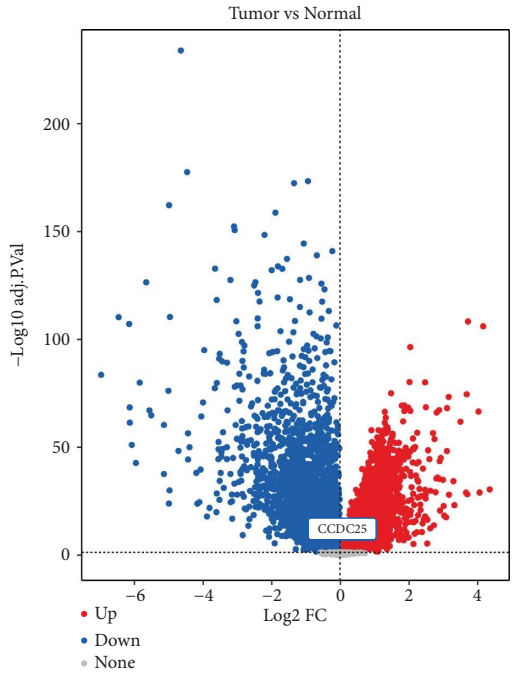

(b)

Figure 2: Continued.

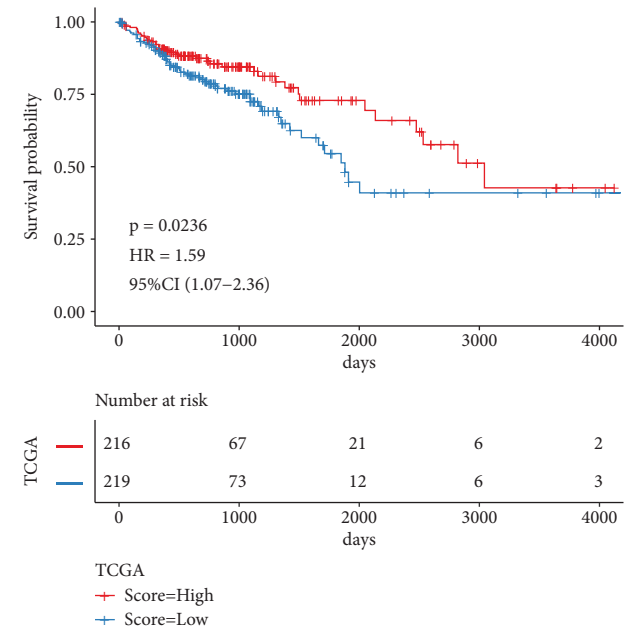

(c)

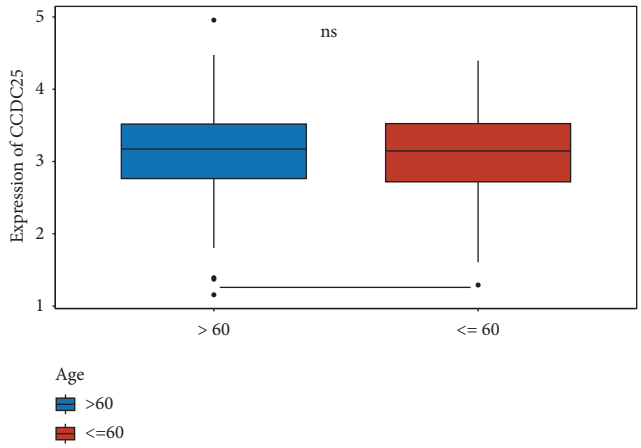

(d)

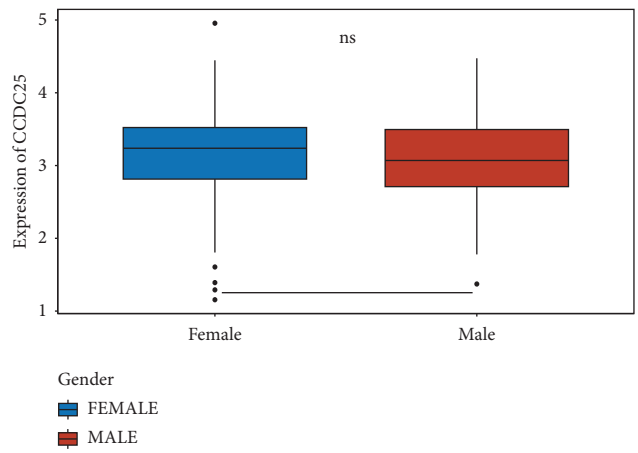

(e)

Figure 2: Continued.

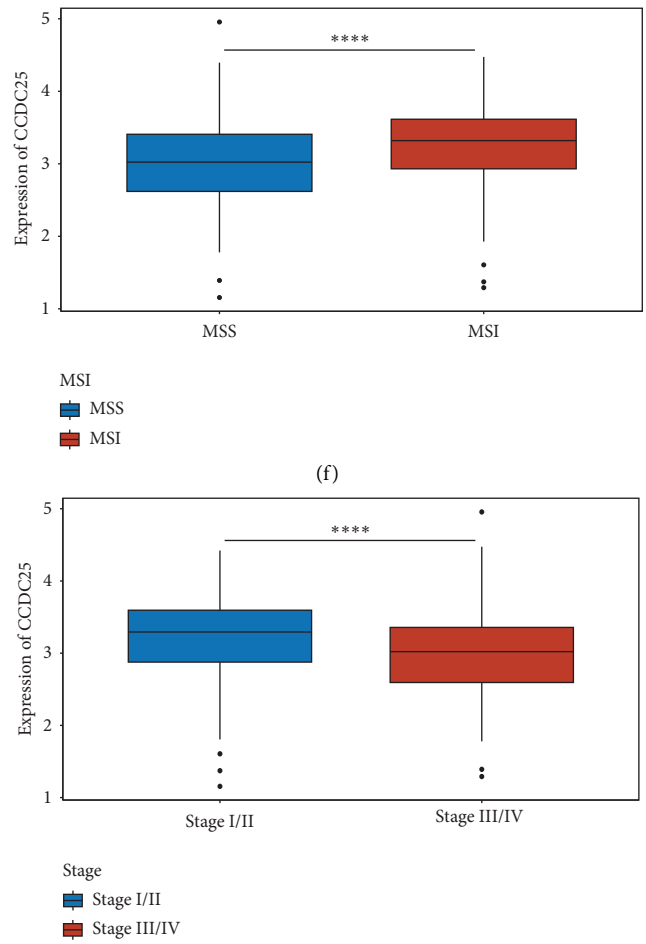

Figure 2: Identification of differentially expressed CCDC25 in CRC. (a) The expression of CCDC25 in pan-cancer TCGA clinical patients based on TIMER 2.0. (b) Volcano plots of DEGs between tumor and normal tissues in the TCGA-COAD cohort. (c) Kaplan–Meier survival analysis of the OS between high-CCDC5 and low-CCDC25 groups in CRC. (d–g) Boxplots of the correlation between CCDC25 expression and clinical characteristics (age, gender, microsatellite stability (MSS)/microsatellite instability (MSI), and stages).

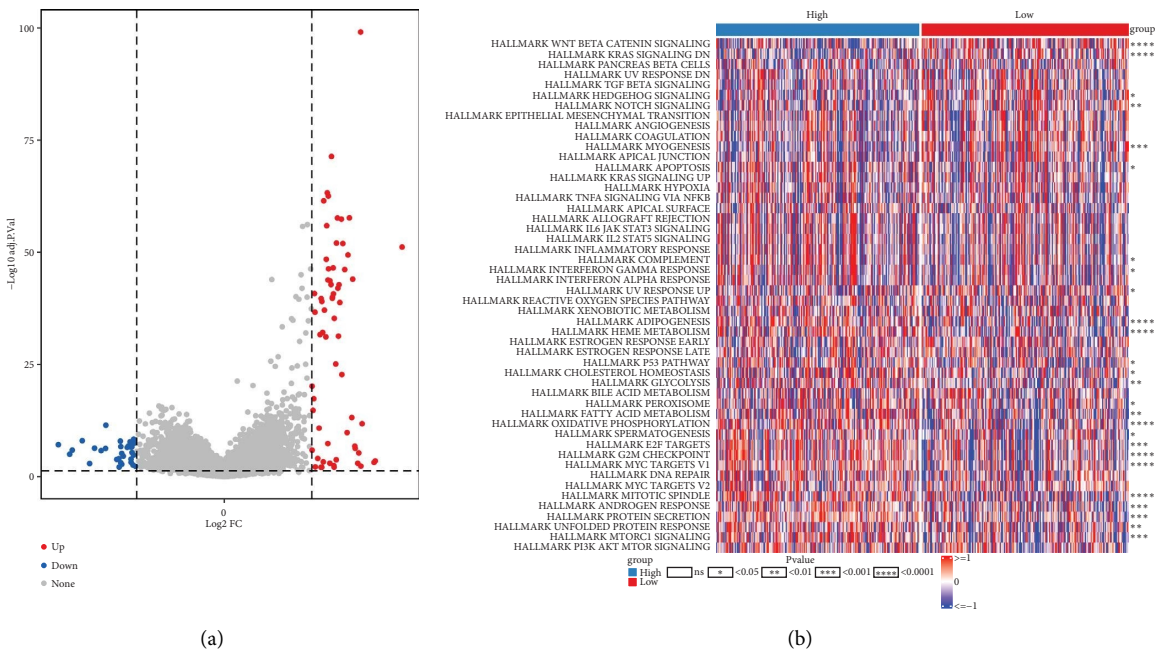

Figure 3: Continued.

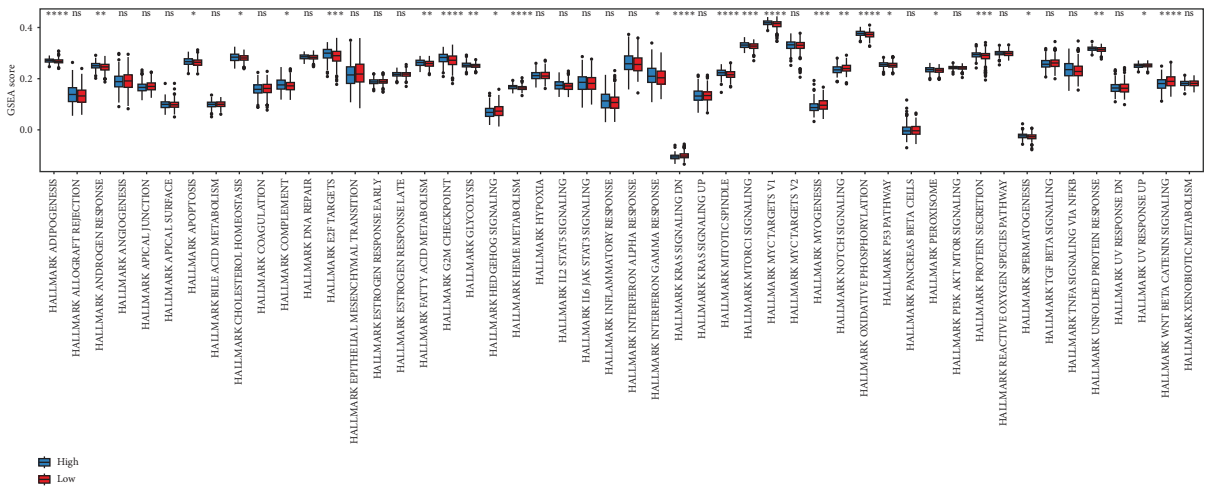

(c)

Figure 3: CCDC25-associated functional annotation and pathway enrichment analysis in CRC. (a) Volcano plots of DEGs between high-CCDC5 and low-CCDC25 groups in the TCGA-COAD cohort. (b) Heatmap of biological function analysis between high-CCDC5 and low-CCDC25 groups in CRC using GSEA. (c) Boxplots of the different enrichment of pathways between high-CCDC5 and low-CCDC25 groups.

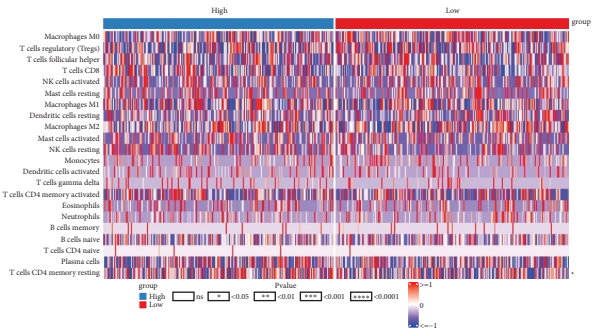

(a)

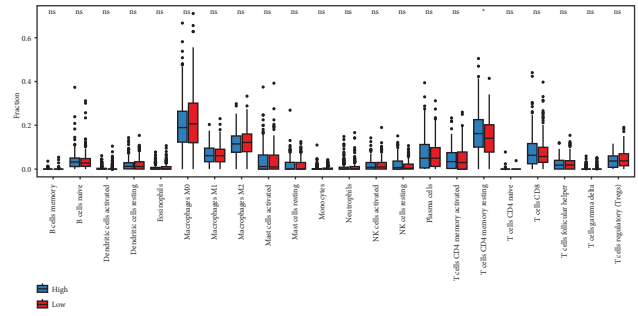

(b)

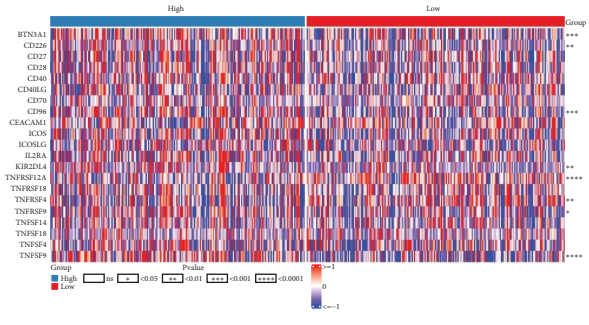

(c)

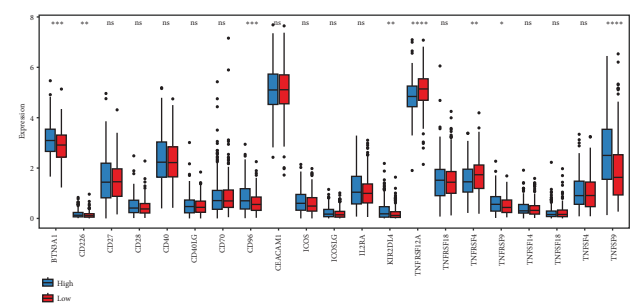

(d)

Figure 4: Continued.

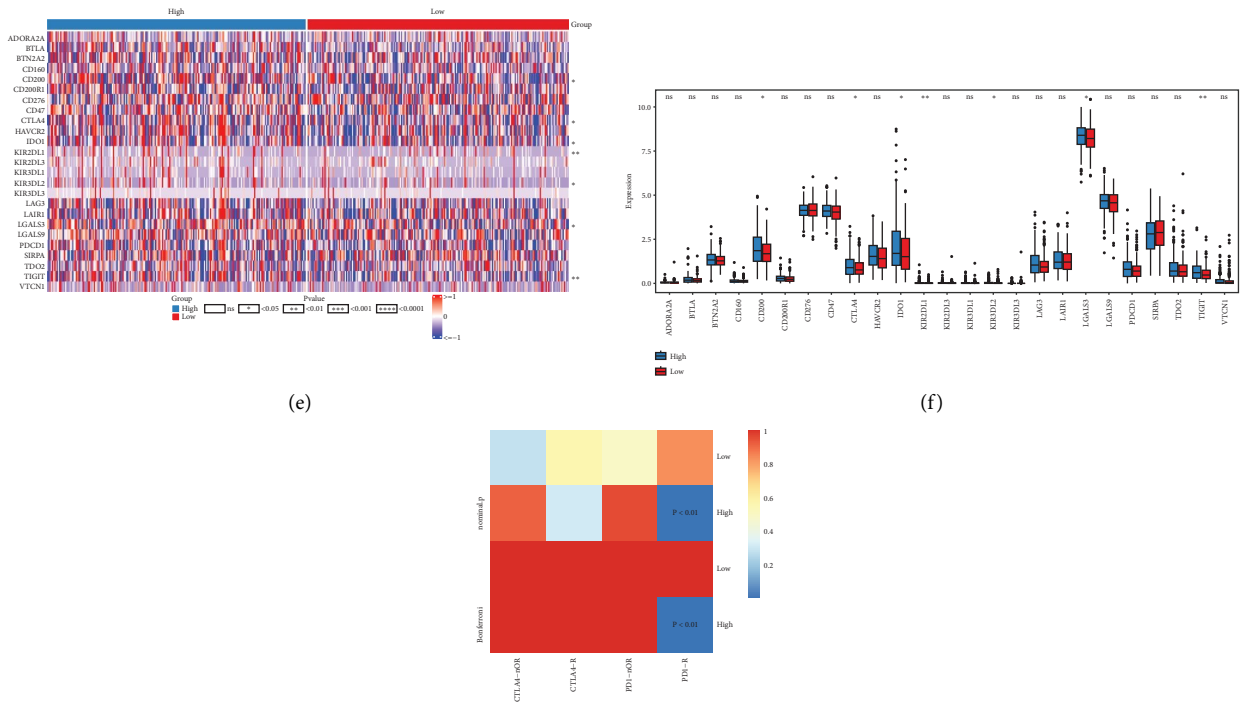

(e) (f) (g)

Figure 4: CCDC25-associated immune cell infiltration and immunotherapeutic response in CRC. (a) Heatmap of immune cell infiltration in TME between high-CCDC5 and low-CCDC25 groups. (b) Boxplots of differences in infiltrated immune cells between high-CCDC5 and low-CCDC25 groups. (c, e) Heatmap of differentially expressed immune checkpoints between high-CCDC5 and low-CCDC25 groups. (d, f) Boxplots of differentially expressed immune checkpoints between high-CCDC5 and low-CCDC25 groups. (g) Submap analysis for prediction of response to anti-PD1 or anti-CTLA4 immunotherapy in patients with high-CCDC5 and low-CCDC25 expressions (author anonymous).

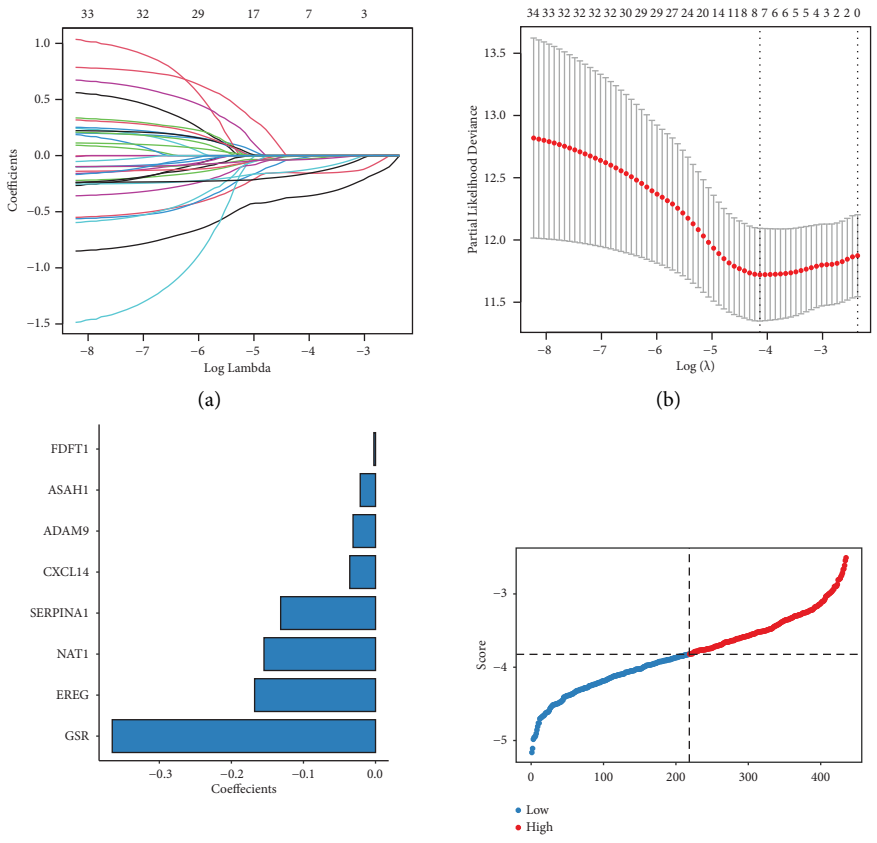

(a) (b) (c) (d)

Figure 5: Continued.

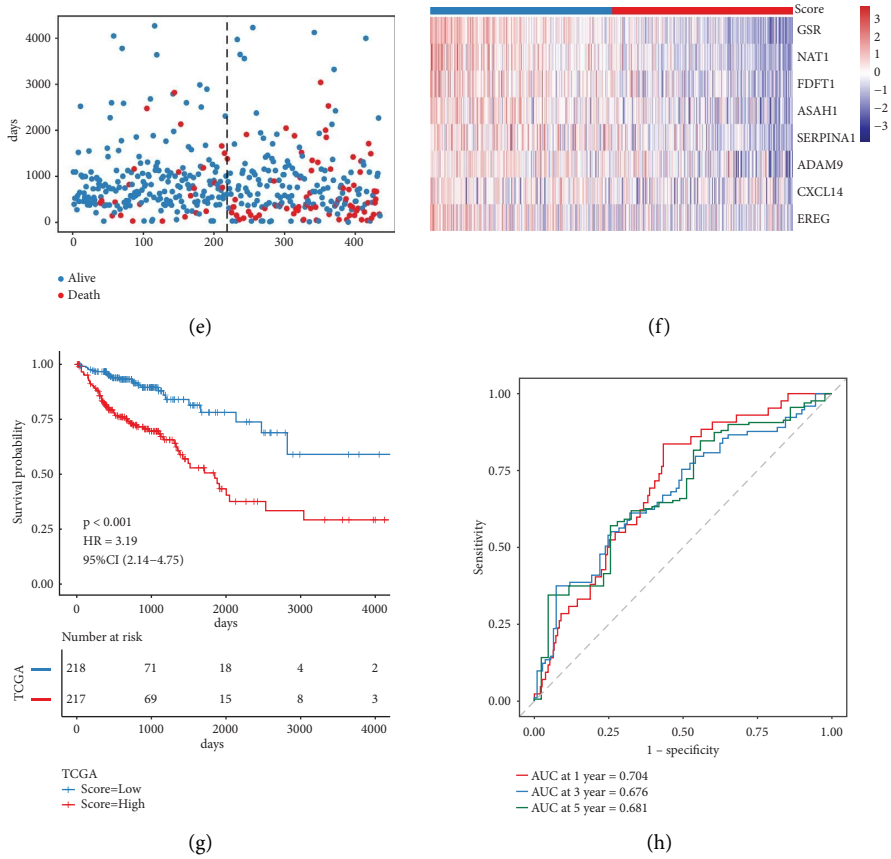

Figure 5: Construction of a CCDC25-associated prognostic model of CRC. (a, b) LASSO Cox analysis identified the eight prognostic CCDC25-associated genes in the TCGA-COAD cohort. (c) Histogram of the eight prognostic genes and corresponding coefficients in the TCGA-COAD cohort. (d) The rank of the risk score in the TCGA-COAD cohort. (e) The distribution of the risk score and survival time in the TCGA-COAD cohort. (f) The heatmap of expression of patterns of eight prognostic genes between high-risk and low-risk groups. (g) Kaplan–Meier survival analysis of the OS between high-risk and low-risk groups. (h) ROC curves and the AUC values of the 1-, 3-, and 5-year OS of patients from the TCGA-COAD cohort.

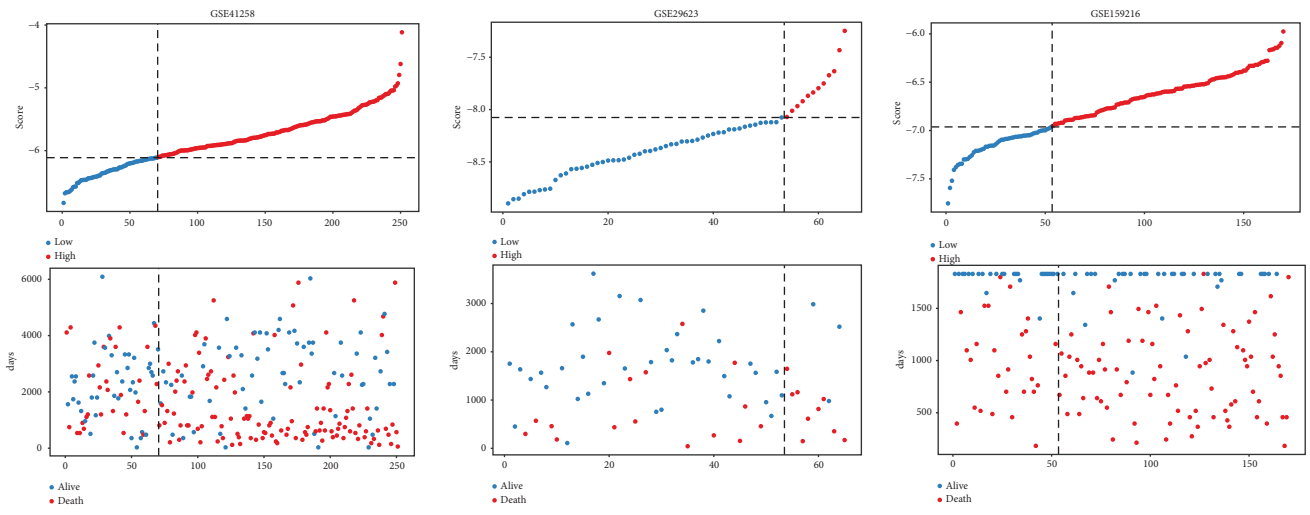

Figure 6: Continued.

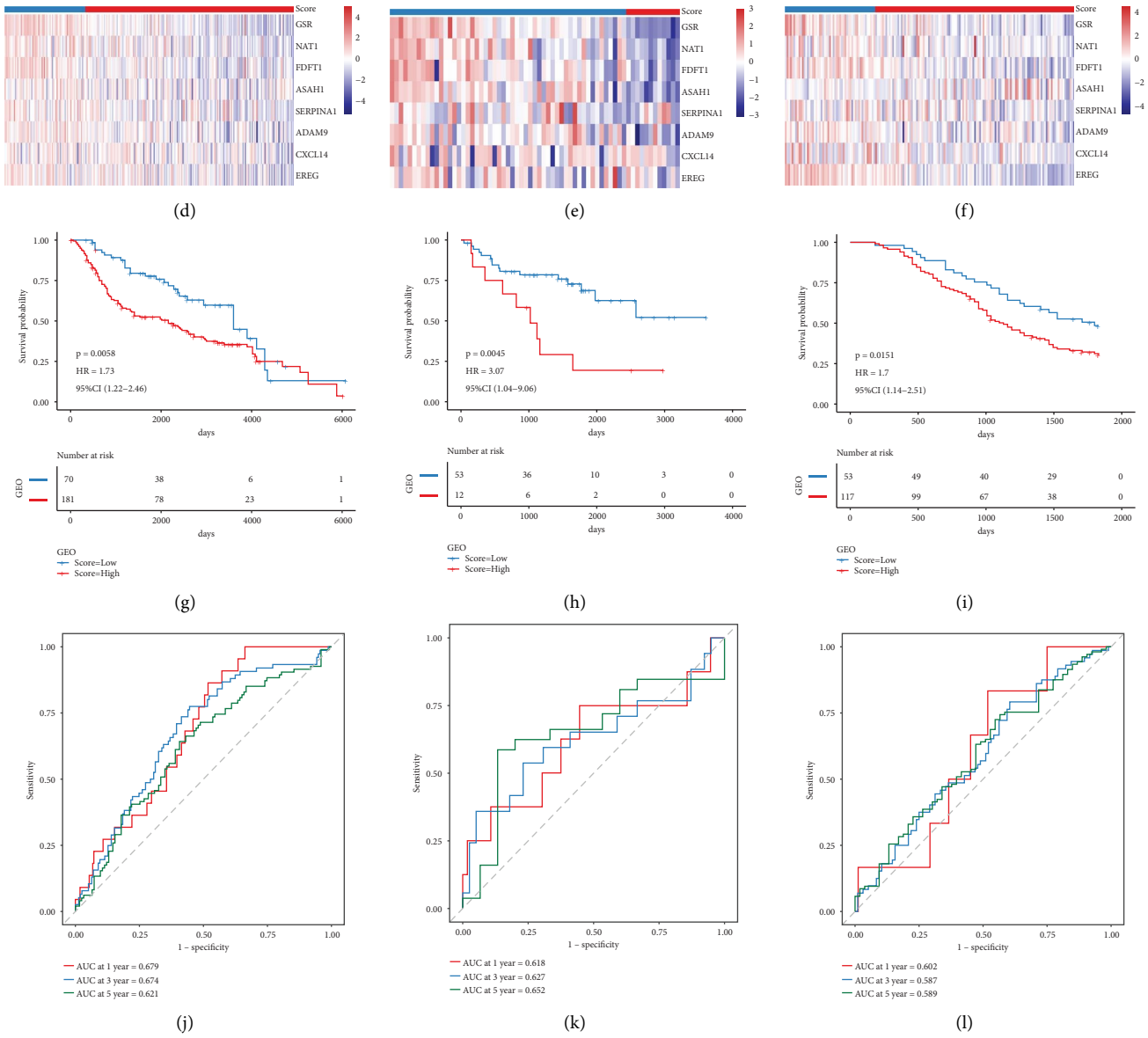

Figure 6: Validation of a CCDC25-associated prognostic model of CRC. (a–c) The rank of the risk score in the GSE41258, GSE29623, and GSE159216 cohorts, respectively. (d–f) The distribution of the risk score and survival time in the GSE41258, GSE29623, and GSE159216 cohorts, respectively. (g–i) Kaplan–Meier survival analysis of the OS between high-risk and low-risk groups in the GSE41258, GSE29623, and GSE159216 cohorts, respectively. (j–l) ROC curves and the AUC values of the 1-, 3-, and 5-year OS of patients from the GSE41258, GSE29623, and GSE159216 cohorts, respectively.

3.6. Development and Evaluation of a CCDC25-Associated Predictive Nomogram. Finally, the risk score and clinical characteristics (stage and age) were identified as independent factors by multivariate Cox analysis (Figure 7(a)). Subsequently, a nomogram was constructed based on the independent factors (Figure 7(b)). The AUC values of ROC curves for 1-, 3-, and 5-year survival prediction were 0.77, 0.792, and 0.78, respectively (Figure 7(c)). The calibration curve showed the accurate prediction ability for the 1-, 3-, and 5-year survival prediction (Figure 7(d)). The DCA curves revealed the higher net benefit of a decision based on a nomogram compared to individual predictive factors (Figure 7(e)).

4. Discussion

CCDC25, a plasma membrane-located extracellular DNA sensor involved in NET-mediated metastasis of cancer cells in several solid tumors [29], has been relatively unexplored in CRC. In our study, we initially demonstrated a negative association between CCDC25 expression and CRC risk through MR analysis. Moreover, our pan-cancer analysis revealed significantly decreased CCDC25 expression in tumor tissues compared to normal tissues. This decreased expression correlated significantly with better survival outcomes, MSI status, and early stages of CRC. These findings suggested a potential protective role for CCDC25 in

Multivariate Cox

Variable	HR (95%CI)	P
age (>60 vs. <=60)	2.10 (1.22–3.62)	0.007
stage (Stage III/IV vs. Stage I/II)	3.18 (2.02–5.00)	<0.001
riskgroup (High vs. Low)	2.65 (1.64–4.27)	<0.001
gender (MALE vs. FEMALE)	0.85 (0.55–1.31)	0.453
MSI (MSS vs. MSI)	0.71 (0.46–1.09)	0.117

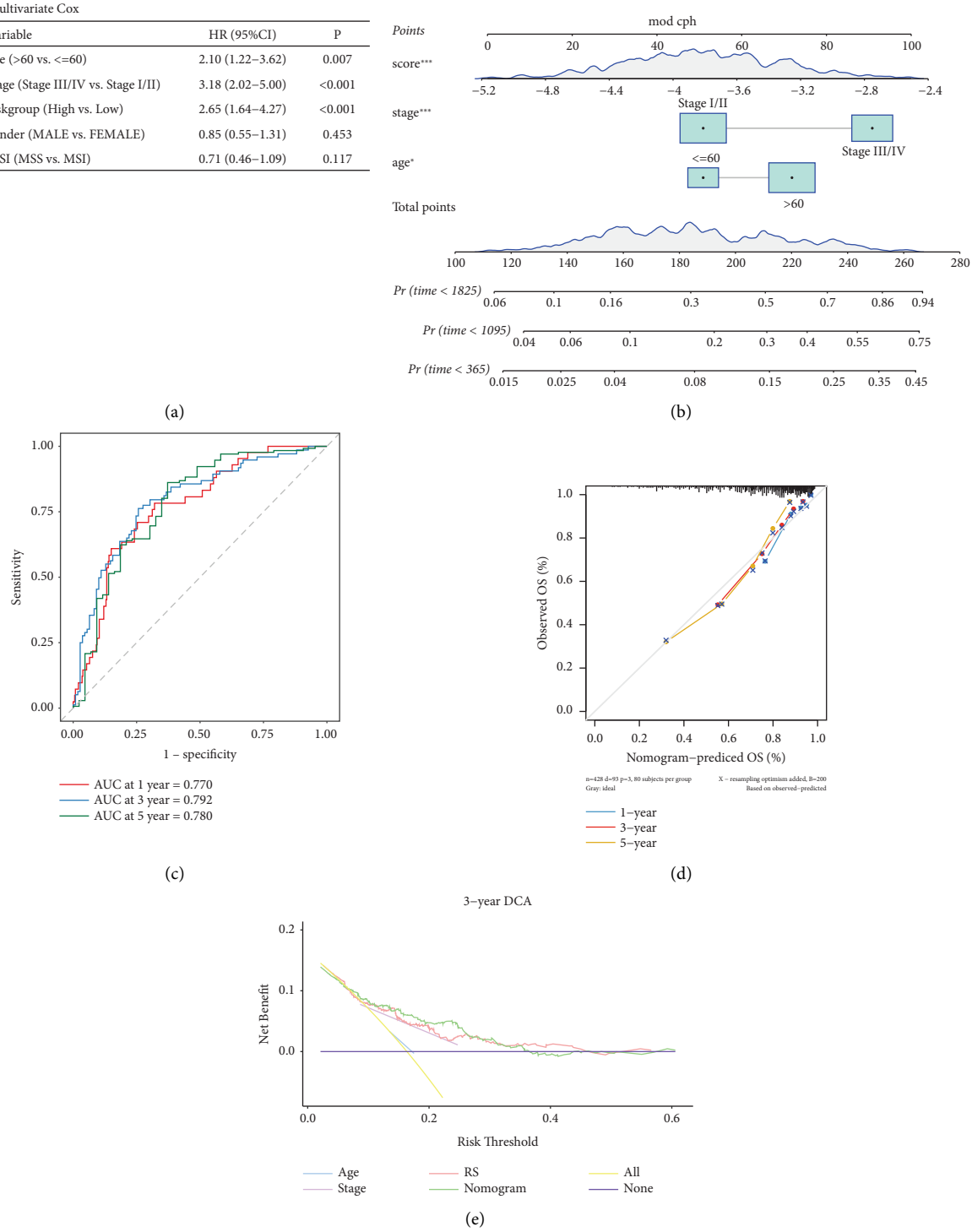

Figure 7: Development and evaluation of a CCDC25-associated predictive nomogram. (a) Multivariate Cox analysis identified the independent factors for survival prediction of CRC. (b) A nomogram was constructed based on independent factors (risk score, stages, and age). (c) ROC curves and the AUC values of the 1-, 3-, and 5-year OS of the nomogram. (d) Calibration curve of the 1-, 3-, and 5-year OS of the nomogram. (e) The DCA curves revealed the benefit of individual predictive factors of the nomogram.

CRC. Our MR analysis further supported that high CCDC25 expression inhibits CRC risk. In addition, survival analysis indicated that patients with high CCDC25 expression experienced better survival outcomes compared to those with low CCDC25 expression.

To validate the protective role of CCDC25 in CRC, we conducted a comprehensive exploration of its expression and its correlations with biological functions, immune cell infiltration, expression of immune checkpoints, and response to anti-PD1 and anti-CTLA4 therapies. CCDC25

expression was found to influence dysregulation of several pathways.

High CCDC25 expression was notably associated with reprogramming of metabolism, such as cholesterol homeostasis, fatty acid metabolism, glycolysis, and oxidative phosphorylation. Previous studies have established that metabolic dysregulation is a hallmark of cancer. Cancer cells alter various metabolic pathways to increase bioenergy and biosynthesis, supporting their proliferation and survival [30, 31]. Here, high CCDC25 expression might be involved in the dysregulation of metabolism reprogramming of CRC to promote tumorigenesis. Conversely, low-CCDC25 expression was associated with the Hedgehog signaling, Notch signaling, and beta-catenin signaling pathways. The hedgehog signaling pathway plays a key role in embryonic development and it is also crucial in the development and metastasis of CRC [32, 33]. Besides, the Notch signaling pathway is involved in many cancers biology and has been found to be activated in CRC [34–36]. The beta-catenin signaling pathway contributes to tumor initiation and progression [37–39]. Here, we found that low CCDC25 expression was involved in canonical cancer-related pathways, suggesting that downregulated CCDC25 might activate the cancer-related pathways and promote dysregulation of metabolism reprogramming in CRC.

We found that high CCDC25 expression was associated with infiltrating resting memory CD4+ T cells. The population of tissue-resident memory CD4 T cells plays a superior protective role against secondary infections [40]. Moreover, we also found differentially expressed immune checkpoints in high/low-CCDC25 expression groups. High CCDC25 expression was associated with increased expression of BTN3A1, CD226, CD96, KIR2DL4, TNFRSF9, TNFSF9, CD200, CTLA4, IDO1, KIR2DL1, LGALS3, and TIGIT, On the contrary, high CCDC25 expression was associated with decreased expressions of TNFRSF12A and TNFRSF4. High expression of CCDC25 exhibited a more sensitive response to anti-PD1 therapy. We next investigated the influences of the CCDC25 expression on the prognosis of CRC. FDFT1, ASAH1, ADAM9, CXCL14, SERPINA1, NAT1, EREG, and GSR were identified as the prognostic gene signature for CRC patients from the DEGs between high-CCDC25 and low-CCDC25 expression groups. FDFT1 is a gene that encodes the membrane-associated enzyme squalene synthase, which plays a crucial role in cholesterol biosynthesis [41]. FDFT1 plays a dual role in different cancers and can be applied as the potential prognostic marker and target for anticancer therapy [42, 43]. FDFT1 has been selected as a prognostic marker for CRC [44, 45], and a high expression of FDFT1 is associated with a better prognosis in the previous study and the present study [46]. ASAH1 has been found to predict lymph node metastasis in breast and colorectal cancers [47, 48] and can be used as the potential biomarker for predicting the treatment outcome of colon cancer [49]. ADAM9 is overexpressed in many cancers, including non-small cell lung, pancreatic, gastric, breast, ovarian, and CRC [50], and cancer-associated fibroblasts (CAFs)-derived ADAM9 is implicated in worse survival in CRC [51]. The chemokine CXCL14 is widely upregulated in many malignancies, including ovarian cancer, [52] oral cavity squamous cell carcinoma [53], glioma [54], prostate cancer [55], and CRC [56, 57]. SERPINA1 also plays an important role in CRC as a novel prognostic biomarker and candidate therapeutic target in CRC [58, 59]. NAT1 has been found to be downregulated and associated with poor prognosis in CRC patients [60]. EREG is one of the EGFR ligands and plays a central role in the development of CRC [61, 62]. GSR is a key enzyme of amino acid metabolism and is associated with the immune escape of CRC [63]. Although our study provides a comprehensive analysis of the regulatory role of CCDC25 in CRC, there are still some limitations. The molecular mechanisms have not been further validated. Therefore, in future studies, we will verify the conclusions of this research through *in vivo* and *in vitro* experiments.

5. Conclusion

In this study, based on GWAS summary statistics and transcriptomic expression files, we first investigated the association between CCDC25 expression and risk of CRC and explored the crucial role of CCDC25 in CRC. These findings suggested that CCDC25 might play a protective role in CRC, and it might be used as a candidate biomarker for diagnosis and treatment of CRC.

Data Availability

Publicly available datasets were analyzed in this study. The GWAS summary statistics were obtained from the publicly available database IEU Open GWAS (https://gwas.mrcieu.ac.uk/datasets/ebi-a-GCST012876/). The eQTL data were extracted from the eQTLGen consortium (https://www.eqtlgen.org/cis-eqtls.html). The TCGA-COAD dataset can be found in The Cancer Genome Atlas (TCGA, https://cancergenome.nih.gov). The GSE41258, GSE29623, and GSE159216 datasets could be downloaded from Gene Expression Omnibus (GEO, https://www.ncbi.nlm.nih.gov/geo/).

Consent

All authors have consent for publication.

Conflicts of Interest

The authors declare that they have no conflicts of interest.

Authors' Contributions

Chunhua Li and Yaping Dong conceived and designed the study, as well as reviewed and edited the article. Guowei Zhang and Yuling Ma wrote the original draft. Jianfeng Shao and Caiping Ke downloaded and analyzed the raw data. Guowei Zhang and Yuling Ma contributed equally to this work.

Supplementary Materials

Table S1: the differentially expressed genes between tumor tissues and normal tissues in the TCGA-COAD cohort. Table S2: the differentially expressed genes between CCDC25 high and low expression groups in the TCGA--COAD cohort. Table S3: univariate Cox analysis of the prognostic genes of the TCGA-COAD cohort. (*Supplementary Materials*)

References

[1] H. Sung, J. Ferlay, R. L. Siegel et al., "Global cancer statistics 2020: GLOBOCAN estimates of incidence and mortality worldwide for 36 cancers in 185 countries," *CA: A Cancer Journal for Clinicians*, vol. 71, no. 3, pp. 209–249, 2021.

[2] R. L. Siegel, K. D. Miller, H. E. Fuchs, and A. Jemal, "Cancer statistics, 2022," *CA: A Cancer Journal for Clinicians*, vol. 72, no. 1, pp. 7–33, 2022.

[3] C. Eng, A. A. Jácome, R. Agarwal et al., "A comprehensive framework for early-onset colorectal cancer research," *The Lancet Oncology*, vol. 23, no. 3, pp. e116–e128, 2022.

[4] E. Dekker, P. J. Tanis, J. L. A. Vleugels, P. M. Kasi, and M. B. Wallace, "Colorectal cancer," *The Lancet*, vol. 394, no. 10207, pp. 1467–1480, 2019.

[5] R. Yamashita, J. Long, T. Longacre et al., "Deep learning model for the prediction of microsatellite instability in colorectal cancer: a diagnostic study," *The Lancet Oncology*, vol. 22, no. 1, pp. 132–141, 2021.

[6] J. Lou, J. Xu, Y. Zhang et al., "PPsNet: an improved deep learning model for microsatellite instability high prediction in colorectal cancer from whole slide images," *Computer Methods and Programs in Biomedicine*, vol. 225, Article ID 107095, 2022.

[7] L. H. Biller and D. Schrag, "Diagnosis and treatment of metastatic colorectal cancer: a review," *JAMA*, vol. 325, no. 7, pp. 669–685, 2021.

[8] S. Roessler, E. L. Long, A. Budhu et al., "Integrative genomic identification of genes on 8p associated with hepatocellular carcinoma progression and patient survival," *Gastroenterology*, vol. 142, no. 4, pp. 957–966.e12, 2012.

[9] X. Cheng, X. Yin, and J. Song, "Integrated analysis of NET-DNA receptor CCDC25 in malignant tumors: pan-cancer analysis," *Health Science Reports*, vol. 6, no. 10, p. e1621, 2023.

[10] L. Yang, Q. Liu, X. Zhang et al., "DNA of neutrophil extracellular traps promotes cancer metastasis via CCDC25," *Nature*, vol. 583, no. 7814, pp. 133–138, 2020.

[11] S. Proungvitaya, W. Klinthong, T. Proungvitaya et al., "High expression of CCDC25 in cholangiocarcinoma tissue samples," *Oncology Letters*, vol. 14, no. 2, pp. 2566–2572, 2017.

[12] R. Chanakankun, T. Proungvitaya, D. Chua-On et al., "Serum coiled-coil domain containing 25 protein as a potential screening/diagnostic biomarker for cholangiocarcinoma," *Oncology Letters*, vol. 19, no. 1, pp. 930–942, 2020.

[13] C. A. Emdin, A. V. Khera, and S. Kathiresan, "Mendelian randomization," *JAMA*, vol. 318, no. 19, pp. 1925-1926, 2017.

[14] L. Xiao, X. Zou, Y. Liang, Y. Wang, L. Zeng, and J. Wu, "Evaluating the causal effects of TIMP-3 on ischaemic stroke and intracerebral haemorrhage: a mendelian randomization study," *Frontiers in Genetics*, vol. 13, Article ID 838809, 2022.

[15] A. I. Hernández Cordero, X. Li, S. Milne et al., "Multi-omics highlights ABO plasma protein as a causal risk factor for COVID-19," *Human Genetics*, vol. 140, no. 6, pp. 969–979, 2021.

[16] B. Guan, M. Yang, X. Shen et al., "Genetically determined serum bilirubin level and the risk of heart failure: a mendelian randomization study," *Frontiers in Genetics*, vol. 14, Article ID 1067146, 2023.

[17] U. Võsa, A. Claringbould, H. J. Westra et al., "Large-scale cis- and trans-eQTL analyses identify thousands of genetic loci and polygenic scores that regulate blood gene expression," *Nature Genetics*, vol. 53, no. 9, pp. 1300–1310, 2021.

[18] J. R. Huyghe, S. A. Bien, T. A. Harrison et al., "Discovery of common and rare genetic risk variants for colorectal cancer," *Nature Genetics*, vol. 51, no. 1, pp. 76–87, 2019.

[19] Y. Long, L. Tang, Y. Zhou, S. Zhao, and H. Zhu, "Causal relationship between gut microbiota and cancers: a two-sample Mendelian randomisation study," *BMC Medicine*, vol. 21, no. 1, p. 66, 2023.

[20] G. Hemani, J. Zheng, B. Elsworth et al., "The MR-Base platform supports systematic causal inference across the human phenome," *Elife*, vol. 7, 2018.

[21] L. Chen, H. Yang, H. Li, C. He, L. Yang, and G. Lv, "Insights into modifiable risk factors of cholelithiasis: a Mendelian randomization study," *Hepatology*, vol. 75, no. 4, pp. 785–796, 2022.

[22] S. Burgess, A. Butterworth, and S. G. Thompson, "Mendelian randomization analysis with multiple genetic variants using summarized data," *Genetic Epidemiology*, vol. 37, no. 7, pp. 658–665, 2013.

[23] J. Bowden, G. Davey Smith, P. C. Haycock, and S. Burgess, "Consistent estimation in mendelian randomization with some invalid instruments using a weighted median estimator," *Genetic Epidemiology*, vol. 40, no. 4, pp. 304–314, 2016.

[24] J. Bowden, G. Davey Smith, and S. Burgess, "Mendelian randomization with invalid instruments: effect estimation and bias detection through Egger regression," *International Journal of Epidemiology*, vol. 44, no. 2, pp. 512–525, 2015.

[25] U.R.A.P.J.a.p.a. Score, Statistical Inference in Two-Sample Summary-Data Mendelian Randomization Using Robust Adjusted Profile Score, 2018.

[26] M. Verbanck, C. Y. Chen, B. Neale, and R. Do, "Detection of widespread horizontal pleiotropy in causal relationships inferred from Mendelian randomization between complex traits and diseases," *Nature Genetics*, vol. 50, no. 5, pp. 693–698, 2018.

[27] T. Li, J. Fan, B. Wang et al., "TIMER: a web server for comprehensive analysis of tumor-infiltrating immune cells," *Cancer Research*, vol. 77, no. 21, pp. e108–e110, 2017.

[28] A. Subramanian, P. Tamayo, V. K. Mootha et al., "Gene set enrichment analysis: a knowledge-based approach for interpreting genome-wide expression profiles," *Proceedings of the National Academy of Sciences of the U S A*, vol. 102, no. 43, pp. 15545–15550, 2005.

[29] R. Liu, E. Zhao, F. Wang, and H. Cui, "CCDC25: precise navigator for neutrophil extracellular traps on the prometastatic road," *Signal Transduction and Targeted Therapy*, vol. 5, no. 1, p. 162, 2020.

[30] I. Martínez-Reyes and N. S. Chandel, "Cancer metabolism: looking forward," *Nature Reviews Cancer*, vol. 21, no. 10, pp. 669–680, 2021.

[31] S. La Vecchia and C. Sebastián, "Metabolic pathways regulating colorectal cancer initiation and progression," *Seminars in Cell & Developmental Biology*, vol. 98, pp. 63–70, 2020.

[32] M. Xin, X. Ji, L. K. De La Cruz, S. Thareja, and B. Wang, "Strategies to target the Hedgehog signaling pathway for

cancer therapy," *Medicinal Research Reviews*, vol. 38, no. 3, pp. 870–913, 2018.

[33] N. Geyer and M. Gerling, "Hedgehog signaling in colorectal cancer: all in the stroma?" *International Journal of Molecular Sciences*, vol. 22, no. 3, p. 1025, 2021.

[34] O. Meurette and P. Mehlen, "Notch signaling in the tumor microenvironment," *Cancer Cell*, vol. 34, no. 4, pp. 536–548, 2018.

[35] A. Tyagi, A. K. Sharma, and C. Damodaran, "A review on notch signaling and colorectal cancer," *Cells*, vol. 9, no. 6, p. 1549, 2020.

[36] R. Jackstadt, S. R. van Hooff, J. D. Leach et al., "Epithelial NOTCH signaling rewires the tumor microenvironment of colorectal cancer to drive poor-prognosis subtypes and metastasis," *Cancer Cell*, vol. 36, no. 3, pp. 319–336.e7, 2019.

[37] Y. Zhang and X. Wang, "Targeting the Wnt/β-catenin signaling pathway in cancer," *Journal of Hematology & Oncology*, vol. 13, no. 1, p. 165, 2020.

[38] N. Krishnamurthy and R. Kurzrock, "Targeting the Wnt/beta-catenin pathway in cancer: update on effectors and inhibitors," *Cancer Treatment Reviews*, vol. 62, pp. 50–60, 2018.

[39] F. Yu, C. Yu, F. Li et al., "Wnt/β-catenin signaling in cancers and targeted therapies," *Signal Transduction and Targeted Therapy*, vol. 6, no. 1, p. 307, 2021.

[40] Y. M. Son, I. S. Cheon, Y. Wu et al., "Tissue-resident CD4(+) T helper cells assist the development of protective respiratory B and CD8(+) T cell memory responses," *Sci Immunol*, vol. 6, no. 55, Article ID eabb6852, 2021.

[41] N. A. Said, C. M. Gould, K. Lackovic, K. J. Simpson, and E. D. Williams, "Whole-genome multiparametric screening to identify modulators of epithelial-to-mesenchymal transition," *Assay and Drug Development Technologies*, vol. 12, no. 7, pp. 385–394, 2014.

[42] M. Kanmalar, S. F. Abdul Sani, N. Kamri et al., "Raman spectroscopy biochemical characterisation of bladder cancer cisplatin resistance regulated by FDFT1: a review," *Cellular and Molecular Biology Letters*, vol. 27, no. 1, p. 9, 2022.

[43] N. T. Ha and C. H. Lee, "Roles of farnesyl-diphosphate farnesyltransferase 1 in tumour and tumour microenvironments," *Cells*, vol. 9, no. 11, p. 2352, 2020.

[44] C. Yang, S. Huang, F. Cao, and Y. Zheng, "A lipid metabolism-related genes prognosis biomarker associated with the tumor immune microenvironment in colorectal carcinoma," *BMC Cancer*, vol. 21, no. 1, p. 1182, 2021.

[45] Y. Shao, H. Jia, L. Huang et al., "An original ferroptosis-related gene signature effectively predicts the prognosis and clinical status for colorectal cancer patients," *Frontiers in Oncology*, vol. 11, Article ID 711776, 2021.

[46] M. L. Weng, W. K. Chen, X. Y. Chen et al., "Fasting inhibits aerobic glycolysis and proliferation in colorectal cancer via the Fdft1-mediated AKT/mTOR/HIF1α pathway suppression," *Nature Communications*, vol. 11, no. 1, p. 1869, 2020.

[47] Y. H. Li, H. T. Liu, J. Xu et al., "The value of detection of S100A8 and ASAH1 in predicting the chemotherapy response for breast cancer patients," *Human Pathology*, vol. 74, pp. 156–163, 2018.

[48] H. Ueo, Y. Takano, T. Matsumura et al., "[Identification of genes that predict lymph node metastasis in colorectal cancer cases]," *Fukuoka Igaku Zasshi*, vol. 104, no. 12, pp. 559–563, 2013.

[49] M. Klobučar, P. Grbčić, S. K. Pavelić, N. Jonjić, S. Visentin, and M. Sedić, "Acid ceramidase inhibition sensitizes human colon cancer cells to oxaliplatin through downregulation of transglutaminase 2 and β1 integrin/FAK-mediated signalling," *Biochemical and Biophysical Research Communications*, vol. 503, no. 2, pp. 843–848, 2018.

[50] J. A. Scribner, S. W. Hicks, K. W. Sinkevicius et al., "Preclinical evaluation of IMGC936, a next-generation maytansinoid-based antibody-drug conjugate targeting ADAM9-expressing tumors," *Molecular Cancer Therapeutics*, vol. 21, no. 7, pp. 1047–1059, 2022.

[51] T. Ao, S. Mochizuki, Y. Kajiwara et al., "Cancer-associated fibroblasts at the unfavorable desmoplastic stroma promote colorectal cancer aggressiveness: potential role of ADAM9," *International Journal of Cancer*, vol. 150, no. 10, pp. 1706–1721, 2022.

[52] X. Li, L. Zhao, and T. Meng, "Upregulated CXCL14 is associated with poor survival outcomes and promotes ovarian cancer cells proliferation," *Cell Biochemistry and Function*, vol. 38, no. 5, pp. 613–620, 2020.

[53] A. Parikh, J. Shin, W. Faquin et al., "Malignant cell-specific CXCL14 promotes tumor lymphocyte infiltration in oral cavity squamous cell carcinoma," *Journal for ImmunoTherapy of Cancer*, vol. 8, no. 2, p. e001048, 2020.

[54] A. Kumar, E. Mohamed, S. Tong et al., "CXCL14 promotes a robust brain tumor-associated immune response in glioma," *Clinical Cancer Research*, vol. 28, no. 13, pp. 2898–2910, 2022.

[55] H. Y. Tian, Q. Liang, Z. Shi, and H. Zhao, "Exosomal CXCL14 contributes to M2 macrophage polarization through NF-κB signaling in prostate cancer," *Oxidative Medicine and Cellular Longevity*, vol. 2022, pp. 1–12, Article ID 7616696, 2022.

[56] J. Zeng, X. Yang, L. Cheng et al., "Chemokine CXCL14 is associated with prognosis in patients with colorectal carcinoma after curative resection," *Journal of Translational Medicine*, vol. 11, no. 1, p. 6, 2013.

[57] J. Zeng, M. Li, J. Y. Xu et al., "Aberrant ROS mediate cell cycle and motility in colorectal cancer cells through an oncogenic CXCL14 signaling pathway," *Frontiers in Pharmacology*, vol. 12, Article ID 764015, 2021.

[58] C. H. Kwon, H. J. Park, J. H. Choi et al., "Snail and serpinA1 promote tumor progression and predict prognosis in colorectal cancer," *Oncotarget*, vol. 6, no. 24, pp. 20312–20326, 2015.

[59] J. Xu, S. Dai, Y. Yuan, Q. Xiao, and K. Ding, "A prognostic model for colon cancer patients based on eight signature autophagy genes," *Frontiers in Cell and Developmental Biology*, vol. 8, Article ID 602174, 2020.

[60] J. Cai, H. Sun, L. Chen et al., "NAT1 is a critical prognostic biomarker and inhibits proliferation of colorectal cancer through modulation of PI3K/Akt/mTOR," *Future Oncology*, vol. 17, no. 19, pp. 2489–2498, 2021.

[61] W. L. Cheng, P. H. Feng, K. Y. Lee et al., "The role of EREG/EGFR pathway in tumor progression," *International Journal of Molecular Sciences*, vol. 22, no. 23, p. 12828, 2021.

[62] E. C. Smyth, K. Khan, and D. Cunningham, "AREG and EREG as predictive biomarkers for RAS wild-type colorectal cancer treated with panitumumab: a fresh approach to an old puzzle," *JAMA Oncology*, vol. 2, no. 5, pp. 578-579, 2016.

[63] M. Jiang, H. Cui, Z. Liu et al., "The role of amino acid metabolism of tumor associated macrophages in the development of colorectal cancer," *Cells*, vol. 11, no. 24, p. 4106, 2022.